International Journal of Precision Engineering and Manufacturing-Green Technology
https://doi.org/10.1007/s40684-019-00090-9

Online ISSN 2198-0810
Print ISSN 2288-6206

REVIEW PAPER

Nanoscale Surface and Interface Engineering of Solid Oxide Fuel Cells by Atomic Layer Deposition

Alireza Karimaghaloo[1] · Junmo Koo[2] · Hung-Sen Kang[1] · Shin Ae Song[3] · Joon Hyung Shim[2] · Min Hwan Lee[1]

Received: 23 May 2018 / Revised: 1 October 2018 / Accepted: 5 November 2018

Abstract
Recently, atomic layer deposition (ALD) has drawn much attention as a suitable tool for fabrication and engineering of high performance fuel cell catalysts and electrodes. Intrinsic merits of ALD enable synthesis of conformal and uniform film even at a sub-nm scale with excellent stoichiometry control and reproducibility. Leveraging the unique characteristics, ALD has proven its promising potential as a solution to achieve two major challenges of solid oxide fuel cell research: sluggish kinetics at low operational temperatures and long-term stability. In this review, recent efforts to address the challenges by the use of ALD-based functionalization of surfaces and interfaces of cell components are discussed.

Keywords Atomic layer deposition · Solid oxide fuel cell · Catalyst · Electrode

1 Introduction

Solid oxide fuel cells (SOFC) have been widely studied as alternative clean power source due to their advantages in terms of fuel flexibility, system simplicity and efficiency [1, 2]. Despite these advantages, their high operating temperature (> 800 °C) has limited their lifetime, cost competitiveness, turn-on/off speed and applicability to small-scale devices [3–5]. Reduction of operating temperature down to intermediate (600–800 °C) or low (< 600 °C) temperature regime, however, results in a dramatic loss of kinetics in both ionic transport and electrode reaction [6–9]. Recently, researchers have addressed the issue of slow ionic transport kinetics of low temperature SOFCs by thinning conventional electrolytes down to few hundreds of nm [2, 5]. In addition, the issue of sluggish kinetics related to electrochemical reaction, especially oxygen reduction reaction (ORR) at the cathode sides, has been tackled by many researchers by developing new materials, making composite or alloys, or modifying the chemical and morphological characteristics of surfaces and interfaces. The overall foci of SOFC research have largely been on the improvement of powering performance while lowering operating temperature. Now, the focus is slowly being shifted to securing true cell stability and long-term durability. The usual factors of degradation include microstructural degradation, poisoning by interconnect materials and fuel impurity, unexpected thermal evolution of material such as surface segregation.

This report is mainly focused on the nanoscale engineering of surface and interfaces of SOFC cell components to address the aforementioned two main challenges: (1) maximizing the kinetics electrode reaction and (2) suppressing the long-term cell degradation during operation. In this vein, major SOFC degradation mechanisms are first summarized and expected benefits of nanoscale engineering are briefed. An introduction of atomic layer deposition (ALD), a rising atomic-scale deposition technique to be proposed as a promising approach of nanoscale engineering in this report, follows. Subsequently, a succinct summary of prior works on nanoscale interface/surface treatment by the use of ALD

Alireza Karimaghaloo, Junmo Koo and Hung-Sen Kang contributed equally to this work.

✉ Min Hwan Lee
mlee49@ucmerced.edu

Joon Hyung Shim
shimm@korea.ac.kr

[1] Department of Mechanical Engineering, University of California Merced, 5200 North Lake Road, Merced, CA 95343, USA

[2] School of Mechanical Engineering, Korea University, 145 Anam-ro, Seongbuk-gu, Seoul 02841, Republic of Korea

[3] Micro/Nano Scale Manufacturing Group, Korea Institute of Industrial Technology, 143 Hanggaulro, Sangnok-gu, Ansan, Gyeonggi Province 15588, Republic of Korea

Published online: 27 February 2019

to address the issues related to the electrodes of SOFCs is provided.

2 Background

2.1 Necessity of Nanoscale Surface and Interface Engineering

2.1.1 Tiny Scale Benefits Catalytic Kinetics

For catalysis per mass and volume, catalysts with a maximized surface area are preferred. As the size of catalyst become smaller, the surface area to volume ratio and thus the proportion of catalytically active low-coordination sites become larger. The size of catalyst also has a direct impact on the catalytic activity itself because the percentage of surface atoms responsible for the catalytic properties increases with decreasing size [10]. One of the most notable examples can be found in the surprisingly high catalytic performance of nano-sized gold towards CO oxidation [11] while gold in bulk has been regarded chemically inert and poorly active as a catalyst [12]. Later, numerous other studies were reported on the size dependency of the gold nanoparticles (NPs) in CO oxidation [13, 14], alcohol oxidation [15], and propylene epoxidation reactions [16]. It was generally observed that the catalytic activity surges below a certain catalyst size, which can be understood from the fact that atoms with low coordination numbers (e.g. vertex and edge atoms) on the surface are mainly responsible for the catalysis [17].

The same analogy applies to the electrodes of SOFCs. For example, the ORR process at the cathode is comprised of multiple steps: adsorption of molecular oxygen on the catalyst surface, dissociation of molecular oxygen into atomic specie-s, surface diffusion of atomic oxygen to the triple phase boundary (TPB), charge transfer reaction and incorporation of oxygen ions into electrolyte. It is known that the overall ORR kinetics is rate-limited by the dissociative adsorption of oxygen on the surface of catalyst, suggesting the importance of securing large surface area of the catalyst. The ideal structure of high surface area would be best made of nanoscale building-blocks.

2.1.2 Thermal Stability for Nanostructured Electrode

The ripening effect significantly reduces active area of an electrode, and thus is detrimental to the catalytic performance and device durability. Therefore, there have been numerous efforts to suppress the ripening of high surface area catalysts and maintain high catalytic performance with a given amount of electrode, often by interfacing with oxide materials at their interfaces. The morphological stability of high-surface-area structure is conditioned by the interaction with the facing oxide and the resulting change in its free surface energy. However, when the interfacial interaction between the electrode and overcoat is weak, the metal will agglomerate to reduce its free energy without being much restricted by the interaction with oxide [18]. To realize a conformal, uniform and strongly-bound overcoat on a nanoscale-structured electrode, it is imperative to achieve a true nanoscale engineering for the oxide overcoat as well.

2.1.3 Surface-Sensitive Kinetics

In addition to the agglomeration suppression effect, an interface with oxides may enhance the kinetics of catalysis. For example, Pd catalysts encompassed by a ceria (CeO_2) shell showed catalytic activities towards methane combustion [19] and hydrogen oxidation [20], significantly enhanced compared to pure Pd-based catalysts, in addition to reinforced thermal stabilities. Catalysis enhancement by oxide support or coating is often understood in view of reactions occurring at the metal/oxide interface or spillover of reactive species onto/from the oxide supports [21]. Lattice strain induced by an interface is also known to have a significant impact on catalytic activities [22].

The reasoning applies to the SOFC electrodes. For example, the surface exchange kinetics, a major factor of overall ORR kinetics, is highly dependent upon the concentration of oxygen vacancy sites on the electrode surface. While all other parameters fixed by having the underlying structure intact, only very surface of electrodes can be engineered accordingly at the atomic-scale or nanoscale to boost the highly surface sensitive kinetics. By keeping the overall underlying structure, we are free of concern on charge transport through the underlying electrode and thermomechanical stability of the structure while improving the surface-sensitive kinetics. The relevant in-depth discussion follows in subsequent chapters of this review.

2.2 Electrode Degradation Mechanism

2.2.1 Sintering/Agglomeration

The usual size of cathodic NPs is on the order of hundred nanometers. However, these high surface area structures are prone to agglomeration (by ripening and coarsening) during high-temperature operation. The rate of agglomeration should be more severe under a high current operation. The degree of agglomeration is expected even more pronounced in noble metal-based electrodes. This agglomeration effect results in a loss of catalytically active surface area and electrode performance over time [11, 12]. The microstructural changes (particle coarsening and densification) results in a decrease of TPB and possible loss of percolation pathway.

In a severe case, it can cause a significant mass transport resistance by hindering fluent oxygen transport.

2.2.2 Segregation

Since early 90's, the surface chemistry of perovskite has been one of the most intense SOFC research topics. Sr segregation has been reported for different perovskite cathode materials including $(La_x,Sr_{1-x})(Co_y,Fe_{1-y})O_{3-\delta}$ (LSCF) [23, 24], and $La_{1-x}Sr_xMnO_{3-\delta}$ (LSM) [25]. It is conjectured that the changes in surface chemistry of cathode by the Sr segregation would have a detrimental impact on the oxygen exchange kinetics. For instance, the high surface polarization resistance associated with oxygen exchange of LSC cathode was attributed to Sr segregation after heat treatment at 600 °C in air for 72 h [26]. Further deterioration of cathodic performance may be originated from the formation of the segregated Sr with surrounding gas phase. Bucher et al. reported a considerable difference in the surface exchange kinetics of LSCF between two different gas environment of dry O_2 and humidified atmosphere [25]. The fivefold higher degradation in the humidified atmosphere was ascribed to the formation of Sr-rich silicate layer in the presence of humidity. However, the impact of Sr segregation on surface kinetics is not yet well understood as some study reports a beneficial impact of Sr segregation. Sase et al. argued an enhanced oxygen surface exchange kinetics is ascribed to an increased oxygen vacancy concentration of LSC caused by Sr segregation [27].

2.2.3 Poisoning

Another major cause of degradation in SOFC is poisoning of the electrode surface. For the cathode, the poisoning is largely originated from Cr deposition at the electrode/electrolyte interface regions or on the surface of electrode and electrolyte. During high temperature operation under oxidizing environment, volatile Cr species such as CrO_3 and $CrO_2(OH)_2$ are generated and deposited on the cell. The deposition readily deteriorate SOFC performance due to the poisoning of cathodes such as LSM and LSCF toward the ORR [28]. The Cr species comes from the usual current collecting interconnects (Fe–Cr alloys) between cells or balance-of-plant components such as heat exchangers.

The poisoning effect is often facilitated with the presence of segregated species exposed on the surface. In many cases, the poisoning species (Cr) have a high tendency to react with segregated cations such as Sr, by forming e.g. $SrCrO_4$. Sr-free materials, such as the Ruddlesden-Popper $La_2NiO_{4+\delta}$ phase would render better resistance against poisoning [29]. It is also noted that an introduction of few ppm of SO_2 can cause a reaction with Sr from the cathode to form $SrSO_4$ and decrease electrode performance [30].

For the anode, both sulfur and carbon are the usual contaminants. Sulfur is always present in every fossil and bio fuels with a ppm variation between few ppm to thousands of ppm. Since sulfur cannot be fully eliminated from these fuels, it is one of the most problematic element deteriorating the long-term performance of a fuel cell [31]. It was widely known that even few ppm of sulfur content can be highly detrimental to the cells. As in most cases for SOFCs, all sulfur compounds are expected to eventually turn into H_2S, the mechanism of sulfur poisoning is considered with H_2S as the main source. With a sufficient O^{2-} supply, H_2S can also act as a fuel [32–34]. However, with a lower supply of O^{2-}, it becomes the source of poisoning. The dissociation reaction leads to an adsorption of sulfur on the surface of catalyst, which blocks fuel access to the catalytically active sites deteriorating the performance. Specifically, on Ni-based anode, the following reaction is considered as major mechanism of deactivation:

$$H_2S(g) \leftrightarrow H_2(g) + S(ads), \tag{1}$$

$$3Ni + xH_2S(g) \leftrightarrow xH_2(g) + Ni_3S_x. \tag{2}$$

As the dissociative adsorption of sulfur is preferred with higher concentration of CO in a fuel, which can be partly ascribed to a preferred adsorption of sulfur on Ni with decreasing H_2 concentration [35]. The sulfidation reaction (i.e. reaction (2)) is known to be less favored with higher temperature, but still shows a negative free reaction energy even at 1000 °C [36]. The poisoning effect can be caused by (a) the blockage of catalytically active sites, (b) a change in reactant adsorption/dissociation kinetics (by a change in electronic landscape) and (c) a reduced diffusion kinetics of reactants and products (by sulfur bonding) [36].

Carbon is another usual contaminant. Coking (carbon formation) on the anode material can occur in various ways. The formed carbon can block the fuel transport, deactivate the surface of catalyst or form filaments that can induce internal stress and cracking of the material. Coking can result in different forms of carbon ranging from graphite to high molecular weight hydrocarbons [37]. It is widely accepted that on metal supported catalysts, hydrocarbons dissociate to atomic carbon and adsorbed on the surface. While this atomic carbon reacts with oxidant to form CO, excessive carbon that does not transform into CO can result in the formation of a polymeric carbon. Similarly, fibers or whiskers and graphitic carbon are produced at a higher temperature range. Polymeric and graphitic carbon can results in the formation of continuous film around the catalysts resulting in its deactivation while whiskers or fiber formation causes the breakdown of the catalysts [38, 39]. There are two different ways of catalyst deactivation when carbon formation occurs on Ni anodes. First, carbon atoms dissolve and diffuse into Ni grains, and become deposited on their outer

surface through the so-called through dissolution–precipitation mechanism. Secondly, the dissolved carbon results in a significant stress inside the Ni grain and eventually cracks the material.

2.3 Atomic Layer Deposition

2.3.1 ALD Basics

A simplified schematic drawing of an atomic layer deposition (ALD) process is given in Fig. 1. A process consists of sequential pulses of gaseous precursors that react with the substrate surface. The first set of precursors are fed into the chamber, adsorbed on the substrate and reacted with the substrate surface. When a precursor is adsorbed on a site that is complete with the same kind of precursor, it will be desorbed from the surface and find another unreacted site. The individual gas-surface reaction is called half-reaction. During each half-reaction, the precursor from a canister is pulsed for a set amount of time and carried to the reaction chamber to allow the precursor to fully react with the substrate surface.

Through this self-limiting process, the coating will be highly precise down to monolayer level. Subsequently, the remaining gaseous precursor and reaction products are purged away from the chamber by a carrier gas. This is then followed by another sequence of pulsing and purging of a counter-reactant precursor (e.g. H_2O, O_2, O_3, NH_3, or other chemical precursor), creating one full layer of the desired material such as metal oxides, sulfides, nitrides or even noble metals. This process is then repeated until a desired film thickness is achieved.

If one is interested in depositing a composite material (such as doped zirconia or doped ceria), the aforementioned pulse-purge-pulse-purge process needs to be performed for each material. For example, the process for Y_2O_3 and the process ZrO_2 need to be alternated to come up with a yttria-stabilized zirconia (YSZ) film. For a stoichiometry control (i.e., control of Y_2O_3 doping ratio), the number of

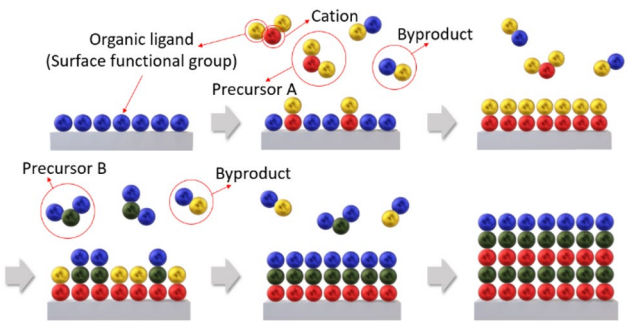

Fig. 1 Conceptual drawing of ALD using self-limiting surface chemistry for an AB binary reaction

Y_2O_3 cycle with respect to that of ZrO_2 cycle is tuned. If the growth rate of the two processes (i.e., the deposition thickness per cycle) were the same, a 1-to-9 ratio between the numbers of Y_2O_3 and ZrO_2 cycles will result in a Y_2O_3 doping ratio of 10 mol %. (Due to a slower deposition kinetics of Y_2O_3 compared to that of ZrO_2, however, a 1-to-9 ratio would result in a lower Y_2O_3 doping.) The one full cycle for YSZ including one Y_2O_3 cycle and a chosen number of ZrO_2 is called a 'super-cycle'. Each cycle for either Y_2O_3 or ZrO_2 is often referred to as a 'sub-cycle'.

ALD processes are mostly performed at < 300 °C, a temperature significantly lower than those needed for conventional CVD processes. Temperatures outside of an optimized window generally result in poor growth rates and non-ALD type deposition [40]. At a too low temperature, reaction kinetics becomes slow and precursor is susceptible to condensation while at a too high temperature, precursors tend to suffer from decomposition or excessive desorption. For each precursors and reactions, the optimum temperature range varies. For this reason, it is desirable to operate ALD within an optimized temperature window to benefit from the merits of ALD.

2.3.2 Merits and Other Characteristics of ALD

The demand for uniform, ultrathin and pinhole-free films originally in semiconductor domain has driven a significant recent advancement of ALD. ALD affords a highly conformal film [41] (continuous adhesion between the deposited film and substrate surface) due to the chemisorption-based deposition [42]. It also enables a sub-nanometer thickness control with excellent film uniformity [41, 43] unlike other alternative deposition techniques such as conventional CVD or physical vapor deposition (PVD; e.g. pulsed laser deposition, sputter deposition). The aforementioned sequential and self-limiting characteristics of ALD enables an unprecedented control over the thickness and uniformity. By utilizing the layer-by-layer deposition nature where each layer deposition is self-limited, the thickness of a film can be tailored by the number of ALD cycles.

A conformal and uniform coating is achievable even on complicated structures of either high aspect ratio or high tortuosity by providing sufficient precursor pulse times so that the precursor can disperse into the structure and undergo complete reactions with the entire surface. In the typical flow reactor setup, precursors are transported into the reaction chamber, and after a deposition process, remaining (unreacted) precursors and byproducts are removed out of the chamber by a carrier gas. In this setup, a highly porous structure with high aspect ratios may not be fully adsorbed with precursor. For extreme nanostructures with high aspect ratio and/or tortuosity, a static ALD reactor, in which the introduced precursors can have sufficient time to fully adsorb

onto the whole surface, may be necessary for a uniform deposition [44].

Another merit of ALD is stoichiometry control. A change in composition is readily achievable by using a different ratio of ALD sub-cycles as described above. However, due to a nonlinear relationship between the cycle ratio and the atomic ratio of resulting film for the ternary oxide processes, a proper recipe development is a necessity for each given system and precursor type.

In addition to these merits, the nature of self-limited layer-by-layer deposition and well-controlled chamber environment also provides an excellent reproducibility largely removing the usual issue of uncontrolled stochastic behavior during thin film deposition. Due to the low operating temperature of ALD, it is also possible to deposit a ceramic or metallic film on a thermally subtle substrate. Possible damage can be further suppressed by employing reactive deposition (e.g. plasma-assisted ALD [45]) where thermal input needed for the reaction is minimized.

On the other hand, the rate of film growth by ALD is intrinsically very low compared to other deposition techniques because of the long process times between layer-by-layer deposition and self-limited reactions per cycle. While the deposition rate varies depending upon chamber temperature, surface chemistry, morphology and the type of reaction, most ALD rates are on the order of 100–300 nm/h [40]. To improve the deposition rate, a new type of ALD, spatial ALD was successfully developed, enabling significant improvement of throughput by a factor of 10–50 [46, 47]. In the spatial ALD mode, a substrate is exposed to spatially-resolved precursor heads unlike the conventional ALD mode where the exposure to a specific set of precursors and reagents was achieved by time-resolved pulsing-purging processes. A spatial ALD has stationary precursor nozzles, under which substrates passes by, enabling deposition rates of ~ 3600 nm/h [48]. The disadvantage of intrinsic low growth rate can be compensated by leveraging its scalability and expandability to parallel processing of multiple depositions. For these reasons, ALD is currently employed by many industries for the mass production of electronic and optical devices [49, 50].

Another major issue with ALD is the high cost of precursors. Furthermore, a considerable amount of precursor introduced into the reaction chamber is purged away without being reacted for deposition, especially in the typical flow reactor-based ALD setup [44]. For electrochemical energy systems where cost competitiveness is a major factor of commercialization, this aspect should be considered rationally. However, as will be detailed in subsequent sections, the usual thickness needed to functionalize the surfaces and/or interfaces of cell components for a significant performance and durability enhancement of SOFCs is not more than few nanometers in most cases, and thus the concern of precursor cost would not be significant in this application. The merits and demerits of ALD are summarized in Fig. 2.

3 ALD for SOFCs

3.1 Overview

ALD has been applied to SOFCs for various purposes. The followings are categorized by the component where ALD is applied: electrolytes, electrode–electrolyte interfaces, cathodes and anodes. The capability of ALD to deposit dense and high-quality films enables a deposition of ultrathin yet gas-tight electrolytes. On the other hand, the capability of coating an ultrathin and uniform oxide over the entire surface area of even a complicated/corrugated structure is leveraged for electrodes and interfaces.

3.2 ALD for Electrolyte

3.2.1 ALD-Based Electrolyte

Considerable efforts were made to decrease ohmic resistances, especially for low temperature SOFCs, either by developing new electrolyte materials or by thinning down the electrolyte to an extreme thickness. Many efforts have been made to demonstrate the so-called micro SOFC (μ-SOFC) with electrolyte thickness of tens-hundreds of nm to counteract the decreased conductivity by thinning down the electrolyte [7, 51–55].

The Fritz group at Stanford pioneered the use of ALD-based electrolyte for low temperature SOFCs [51, 52]. YSZ films were first synthesized by ALD for SOFC purpose [52]. To evaluate ALD YSZ films as an oxide ion conductor,

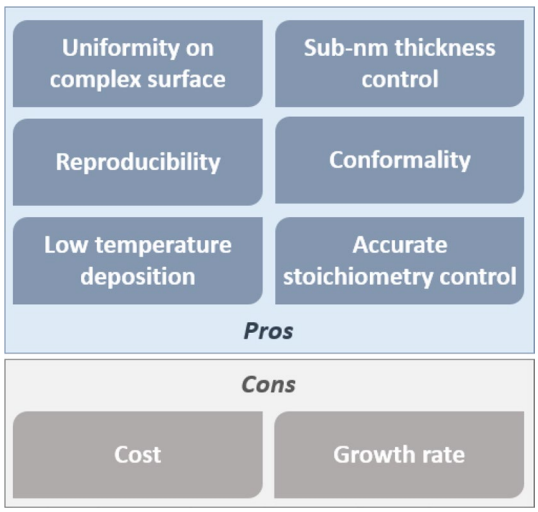

Fig. 2 Merits/demerits of atomic layer deposition

freestanding 60 nm YSZ films were prepared with porous platinum electrodes on both sides of the electrolyte (Fig. 3). They achieved a high power density of 270 mW/cm^2 at 350 °C, which was attributed to low electrolyte resistance and fast electrode kinetics.

By refining the design, a corrugated freestanding fuel cell with a 70 nm thick YSZ membrane was fabricated to increase the electrochemically active surface area (Fig. 4) [51]. The power densities reached a surprising value of 861 mW/cm^2 at 450 °C. In a more recent report, An et al. achieved an even better performance of 1.3 W/cm^2 at 450 °C by nanostructuring 60 nm YSZ electrolyte interposed with a nanogranular catalytic interlayer (YDC) at the cathode/electrolyte interface [56]. The cell exhibited a significant reduction in both the ohmic and polarization losses, which are attributed to a combined effect of employing an ultrathin film electrolyte, enhancement of effective area by 3-D architecture, and superior catalytic activity by the ceria-based interlayer at the cathode.

Despite the excellent powering performance at the extremely low temperatures for SOFCs, the durability of the ALD-based freestanding cell has rarely been studied until very recently. An improved thermomechanical characteristics of freestanding ALD-based cells with an enlarged the cell area was demonstrated by reinforcing edges and corners [57]. The functional stability of the structure was verified by observing a high OCV value of 1.04 V at 350 °C for > 30 h, and the high OCV recovered from the abrupt thermal cycling tests with fast heating and cooling rate of 25 °C/min also confirmed the superior thermal stability. However, the demonstrated durability test is still too short to be acceptable for a practical SOFC device.

In addition to a freestanding setup (where the whole membrane is not mechanically supported by either anode or cathode), there was a recent report that YSZ electrolyte was deposited on a porous anodic aluminum oxide (AAO) substrate [58]. A 70 nm YSZ was deposited by plasma-enhanced ALD (PEALD) to afford a consistently high OCV of 1.17 V at 500 °C (Fig. 5). The thickness was the thinnest among reported on a SOFC supported by a porous substrate.

In another recent report, thin films of yttria-doped ceria (YDC) electrolyte were processed for the first time by ALD for SOFC applications [59]. Interestingly, the as-deposited films were crystalline, well-covered and homogeneous without any need for annealing even though the ALD temperature was not any higher than 350 °C. The ALD-made YDC film exhibited a better dielectric behavior and higher conductivity at > 420 °C compared to a bulk counterpart. However, a full cell test based upon ALD-YDC electrolyte was not reported.

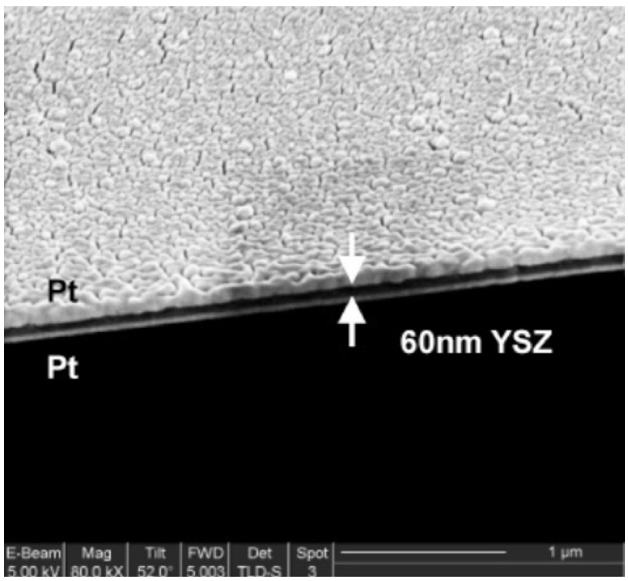

Fig. 3 SEM image of freestanding ALD YSZ films with porous Pt cathode–anode layers. Reproduced with permission from Ref. [52]

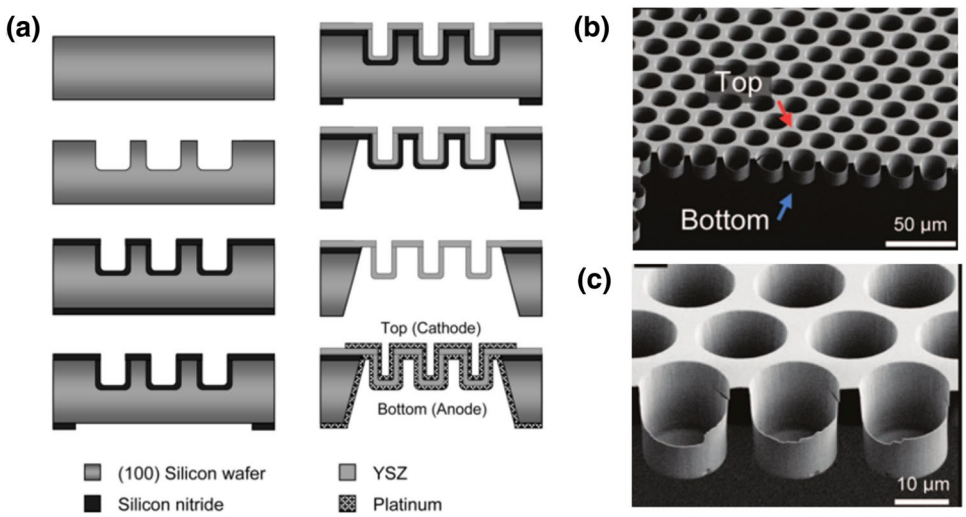

Fig. 4 **a** Schematic drawing depicting the microfabrication process of a freestanding corrugated SOFC. **b**, **c** Cross section of corrugated membrane-based Pt/YSZ/Pt cells. Reproduced with permission from Ref. [51]

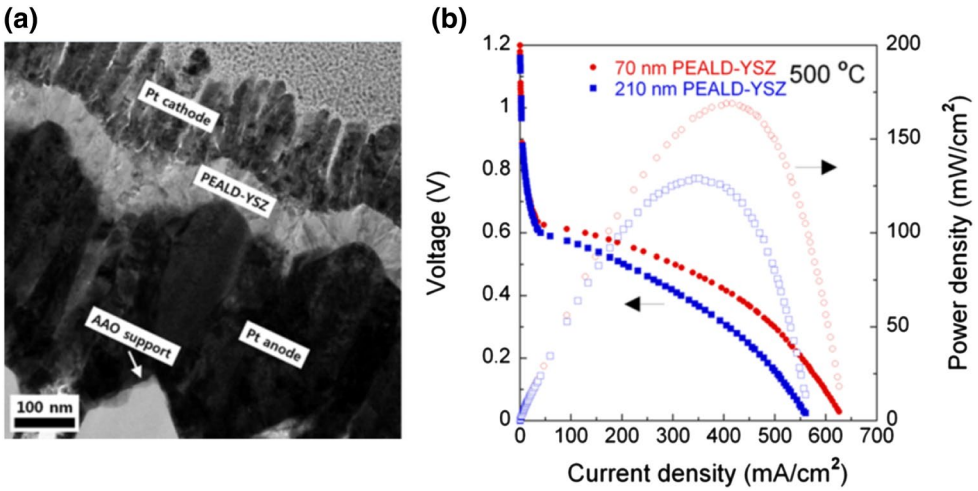

Fig. 5 **a** High-resolution transmission electron microscopy cross-sectional images of 70 nm PEALD- YSZ electrolyte-based cell on an AAO-supported cell. **b** Polarization curves of PEALD-YSZ-based cells at 500 °C with 70 nm and 210 nm YSZ thickness. Reproduced with permission from Ref. [58]

In addition to the conventional SOFCs with an oxygen ion conducting membrane, those with proton-conducting electrolytes recently attract significant attraction as an alternative approach of realizing truly durable ceramic fuel cells with excellent performance [60–62]. Shim et al. first implemented a freestanding proton-conducting fuel cell by depositing 130 nm yttrium-doped $BaZrO_3$ (BZY) by ALD to achieve 136 mW/cm^2 at 400 °C, the highest power density reported at the operating temperature back them [63]. A similar approach (BZY-based freestanding μ-SOFC) was taken by Li et al. to achieve even higher performance of 445 mW/cm^2 at 425 °C by inserting an 8 nm-thick GDC [64].

3.3 ALD for Electrolyte–Electrode Interfaces

3.3.1 Anodic Interface of Electrolytes

As mentioned above, a decent electrolyte thickness (> micron) needs to be provided to secure the mechanical integrity in a usual SOFC setup. However, there are significant room to improve in terms of ohmic resistance. Unfortunately, a true alternative to doped zirconia as an SOFC electrolyte material satisfying both performance and stability has not been identified. A doped zirconia of micron-scale thickness will cause a significant ohmic loss at a reduced operating temperature.

Ceria-based electrolytes are known to exhibit much better ionic conductivities than zirconia counterparts. However, when they are exposed to a reducing environment during high-temperature operation (> ~ 600 °C), the fluorite-structure tends to be reduced, turning into a metallic phase over time. In addition, the volumetric expansion can be caused by the replacement of Ce^{4+} ions (with an ionic radius of 0.97 nm) with larger Ce^{3+} ions (with an ionic radius of 1.14 nm) during the reduction process, also facilitating a deterioration of the mechanical integrity of the cell.

In order to minimize the ohmic resistance while satisfying the minimum thickness requirement, one can consider a bi-layered electrolyte, in which a doped-ceria comprises the majority of electrolyte thickness but is covered by a chemically stable doped-zirconia at its anode interface. The YSZ/GDC bi-layered electrolyte has been arguably one of the most popular approaches among various bi-layer schemes [65–67]. Since few micron-thick YSZ was used, however, a considerable ohmic resistance resulted. Recently, GDC/YSZ bilayer was successfully implemented by having an ultrathin and dense YSZ deposited on GDC via ALD [68]. The thin YSZ film serves as a protective layer against chemical degradation of ceria in a reducing gas environment.

There are several requirements to meet for obtaining a high-performance protective layer. Although a thinner YSZ layer is preferable for minimized ohmic loss, there are limitations as to how thin the YSZ film can be and still serves as a protective layer. The limitation is partially imposed by the onset of material inter-diffusion and significant morphological changes during the high temperature sintering processes. In addition, a pinhole-free and dense layer is also needed to prevent a direct permeation of fuel gas. High film conformality would suppress the formation of "hot spots" where electrical current is concentrated and/or ceria reduction is facilitated. The thickness is also fundamentally limited by the charge conservation criterion to maintain the YSZ stay in the "electrolytic domain" [69]. It is demonstrated that only 28 nm of YSZ (given a YSZ/GDC thickness ratio of 6.5×10^{-5}) stabilized the GDC electrolyte (Fig. 6) [68] while a 25 nm thick YSZ deposited by a sputter deposition process could not provide the chemical stability even with a much higher YSZ/GDC thickness ratio of 1.8×10^{-5} [70]. The ALD approach is an excellent choice to meet all these requirement as it can provide pinhole free and dense layers with high conformality, superior step coverage and accurate thickness control capabilities [41, 71].

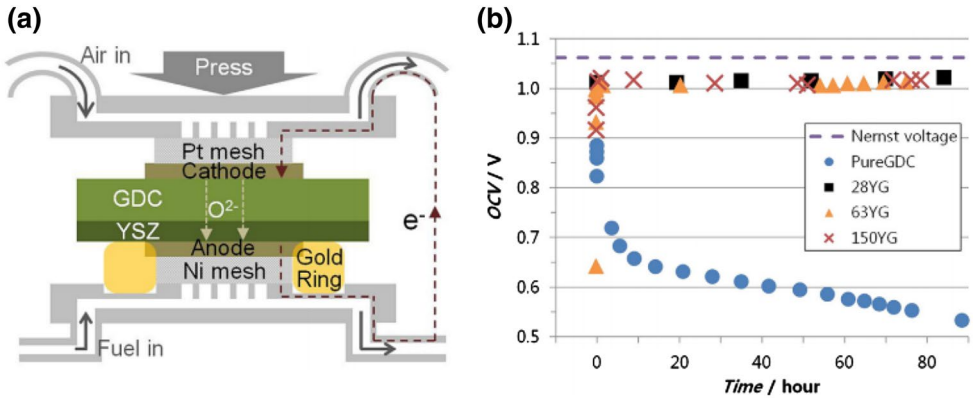

Fig. 6 **a** A schematic diagram depicting the cross-sectional experimental setup. Image is not to scale. **b** Time evolution of OCV under dry H_2 at 600 °C for the pure GDC (blue circle), 28 nm YSZ/GDC (black rectangle), 63 nm YSZ/GDC (yellow triangle) and 150 nm YSZ/GDC (red cross) cells. Reproduced with permission from Ref. [68]

3.3.2 Cathodic Interface of Electrolytes

While YSZ is considered as the most common electrolyte material for SOFCs, its slow oxygen exchange kinetics is a critical drawback of the material. Oxygen exchange coefficient is a measure of neutral oxygen exchange flux across the surface of an electrolyte, which is highly dependent upon the availability of surface oxygen vacancy. The kinetics of sub-processes including surface exchange, charge transport and redox reactions make a combined contribution to the overall ORR kinetics. However, an optimum condition for a sub-process is not necessarily a best condition for other sub-processes. For example, ~ 8 mol % yttria doping in YSZ is known to render the highest ionic conductivity, but the composition may not provide an optimum oxygen incorporation sites for ORR. It was indeed reported that there is a quasi-linear relationship between the surface vacancy concentration and oxygen surface exchange coefficient [72, 73]. Therefore, only the very surface of YSZ can be modified to incur more oxygen vacancies while keeping the underlying bulky YSZ as-optimized for fast ionic transports. Alternatively, one can consider an ultrathin coating of a totally different material with a much higher oxygen exchange kinetics and catalytic performance. It should be a worthwhile approach to modify the stoichiometry and material of the very surface for a better overall ORR kinetics.

As was the case for the earlier section on ALD-based electrolyte, a modification of interfacial characteristics at the electrolyte-cathode interfaces were largely presented by the Prinz group [56, 74–78]. First, Chao et al. performed a parametric study about the impact of surface modification on ORR kinetics [74]. They modified the surface of conventional YSZ substrate by adding a very thin (1 nm) YSZ with different yttria doping ratio via ALD, and measured the resulting electrochemical performance. The yttria doping ratio was simply controlled by changing the ratio of Y and Zr pulsing during ALD (Fig. 7a). From the study, it was found that a merely 1 nm interfacial layer of

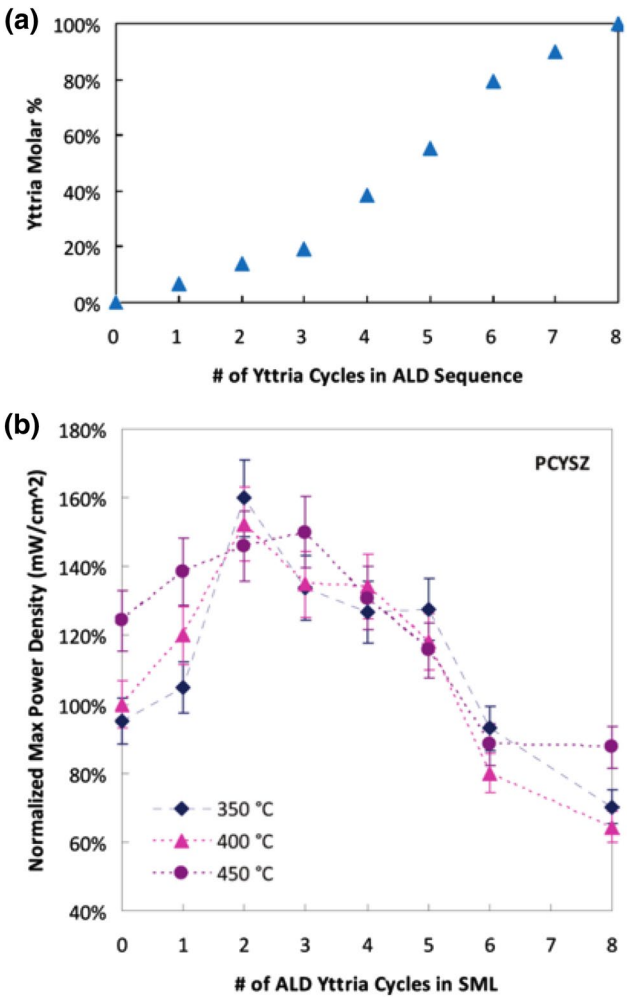

Fig. 7 **a** Relationship between number of yttria cycles during ALD versus yttria molar percentage in the YSZ interlayer. **b** Normalized power density as a function of yttra doping ratio of interlayer sitting on a polycrystalline YSZ. Reproduced with permission from Ref. [74]

YSZ with 14–19 mol % yttria doping improved the powering performance by ~ 50% (Fig. 7b).

Later, Fan et al. demonstrated a significantly enhanced performance of YSZ electrolyte-based SOFC by using a doped ceria interlayer instead of YSZ [77]. Ultrathin YDC layers were added by ALD, in which the doping concentrations of Y_2O_3 were also tuned by changing the Ce:Y pulsing ratios. The powering performance was enhanced by up to ~ 3.5 times, depending on the operational temperature (300–500 °C) within the Y_2O_3 doping window of 12–17 mol % (Fig. 8). The enhanced performance was attributed to an increased oxide ion incorporation rate at the electrode/electrolyte interface. They further studied the impact of YDC interlayer thickness on performance [76]. YDC films of various numbers of ALD super-cycles, ranging from 2 to 35, are inserted into a fuel cell with a 200 µm thick YSZ electrolyte. This optimal YDC interlayer condition (10 super-cycles; 6:1 Ce:Y for each sub-cycle) is applied to a fuel cell test, and the average performance enhancement factor was 1.4 at the operating temperatures of 400 and 450 °C. A power density of 1.04 W/cm^2 at 500 °C is also achieved with the optimal YDC recipe.

An et al. tried a similar approach: an insertion of YDC between an ALD-based YSZ and Pt cathode, but this time, in a freestanding setup [56]. As mentioned above, they achieved a stellar performance of 1.3 W/cm^2 at 450 °C by a significant reduction of ohmic resistance (ultrathin YSZ electrolyte) and the interface treatment by ALD-YDC.

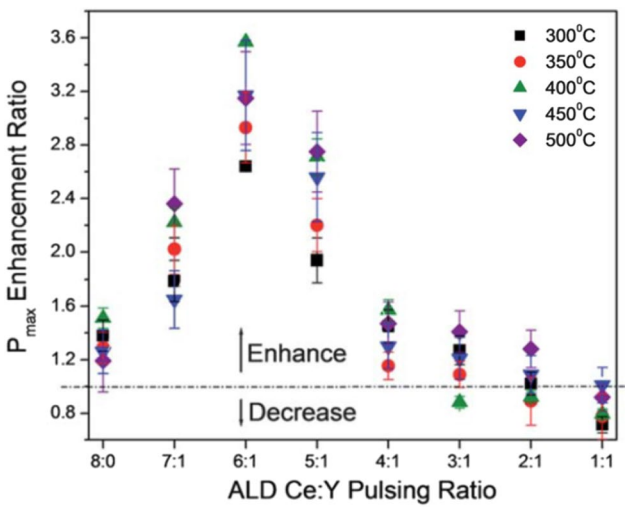

Fig. 8 Power density enhancement ratio as a function of Ce:Y ALD pulsing ratio with polycrystalline YSZ substrates. Reproduced with permission from Ref. [77]

3.4 ALD for Cathodes

The initial motivation toward ALD treatment of cathodes resides in the fact that the optimum sintering temperature of perovskite-based cathodes are significantly lower than the temperature for electrolyte materials. A high sintering temperature results in a larger grain size of the electrode decreasing the electrochemically active area. This is a major drawback of high temperature sintering along with the undesired formation of zirconates [79–81]. The downside of low-temperature sintering is that the adhesion and interconnectivity between particles are weak, which could lead to poor charge transport and mechanical integrity. Therefore, it is important to optimize the microstructure by controlling the grain size and ensuring strong adhesion between particles and different layers simultaneously. As the thermal expansion coefficient and the rate of shrinkage during sintering is usually much higher in perovskites than electrolyte materials, a sintering process with perovskite-based electrodes on top of an electrolyte often causes a significant thermal stresses and sometimes thermo-mechanical defects in the form of delamination and/or crack-development. However, a decoration of catalytically active perovskite NPs on top of a porous electrolyte backbone (as opposed to a deposition of perovskite 'film') would resolve this issue.

On the other hand, the performance of a SOFC is usually limited by the cathodic kinetics especially when the cell is operated at a relatively low temperature. The cathodic ORR reaction is mostly limited by the kinetics of dissociative adsorption or surface transport of electroactive oxygen, as opposed to ionic transport, intense efforts have been made to enlarge the catalytically active surface area of cathodes. ALD treatment is likely to achieve this as the so-called wet impregnation (i.e. infiltration) process does. In addition, the use of ALD treatment can be found in suppressing the materials' susceptibility to changes of surface chemistry by e.g. Sr segregation. Application of a continuous coating is predicted to reduce the segregation, and some studies verified the prediction by infiltration process [82, 83].

Figure 9 lists these effects on the cathodic characteristics that can be expected by an ALD overcoat. First, the high-surface-area electrodes (both anode and cathode) are susceptible to agglomeration/sintering during operation, losing its surface area, and thus its area specific powering capability. An ultrathin oxide overcoat is expected to deter both Ostwald ripening and coalescence of NPs (Fig. 9a). Secondly, an atomic-scale overcoat may modify the kinetics of dissociative adsorption of reactants, catalytic activity, ion incorporation kinetics and/or atomic/ionic transport kinetics as verified from a specific cathodic systems (Fig. 9b). Lastly, an ultrathin overcoat also may thermodynamically stabilize spatial chemistry, and thus suppress segregation of dopants, one of the usual electrode degradation mechanism (Fig. 9c).

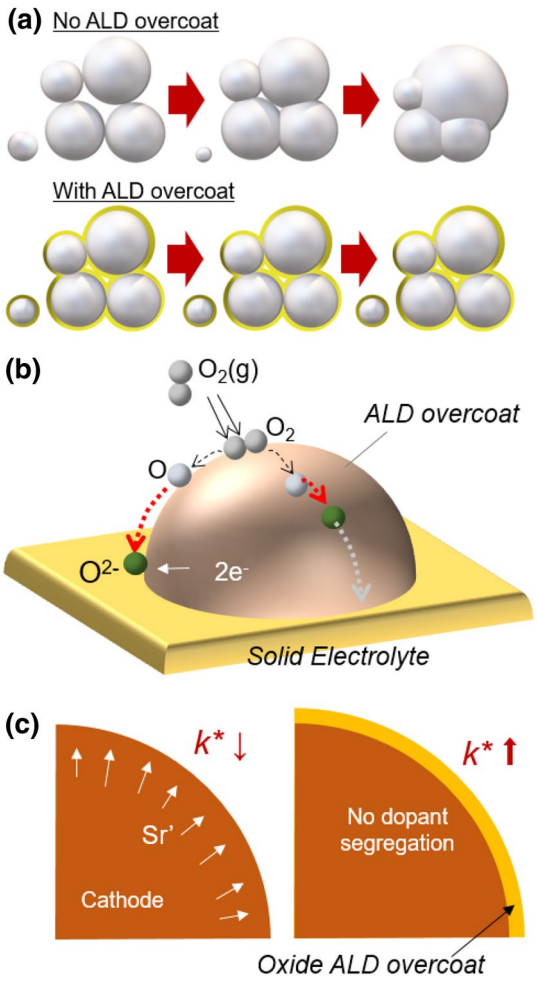

Fig. 9 Major expected roles of ALD-based overcoat on SOFC electrodes. **a** Suppression of particle growth during sintering. **b** Facilitation of dissociative adsorption, transport of neutral and/or ionic species on the surface, and/or charge transfer reaction kinetics. **c** Suppression of Sr segregation

There are other expected benefits of ALD-based treatments such as suppression of impurity poisoning. More details on its impact on both anode and cathode are provided below.

3.4.1 For Noble Metal Cathodes

The self-limiting nature of ALD deposition offers atomic-scale thickness control and enables highly uniform and conformal films with excellent reproducibility [84]. In our recently study, an ultrathin layer of YSZ was coated on a highly porous Pt cathode by ALD to suppress Pt agglomeration for low temperature SOFCs [85]. Even a few nm thick coating was found to suppress the morphological degradation of nano-porous Pt as shown in Fig. 10, which was confirmed by other researchers as well [86, 87]. The coating was expected to retard the Ostwald ripening process by blocking the diffusion of Pt atoms and/or to impede the coarsening

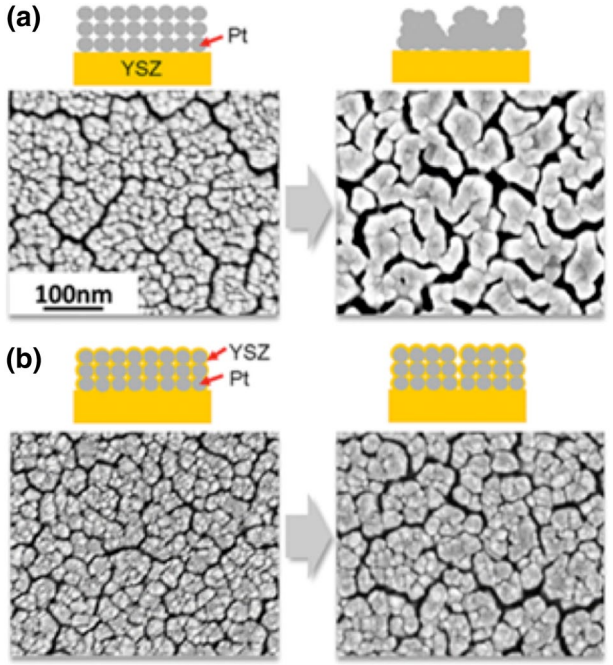

Fig. 10 Morphological change after exposing Pt nanostructure at 500 °C for 20 h without (**a**) and with **b** a nano-thin oxide coating, showing the effectiveness of oxide coating in suppression of agglomeration. Reproduced with permission from Ref. [85]

process by separating each nano-grain from its neighboring grains.

In addition to the suppression of the agglomeration effect, the nanoscale overcoat was also found to enhance the catalytic activity toward ORR even if the oxide is expected to cover (and thus deactivate) part of catalytically active Pt surface. An as-deposited ALD overcoat is uniform, but, the overcoat transforms into an interconnected network of agglomerates or nano-islands (Fig. 11), which provides openings for O_2 gases to have direct access to the Pt surface. In this view, the enhanced ORR kinetics is initially ascribed to an increased TPB.

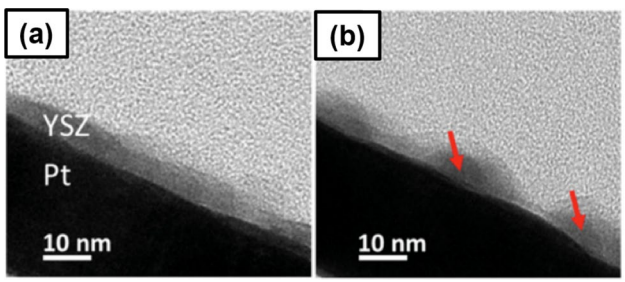

Fig. 11 Cross-sectional TEM images of a YSZ-coated Pt film **a** before and **b** after an annealing at 600 °C for 10 h. A thermally induced agglomeration of YSZ coating is observed. Reproduced with permission from Ref. [85]

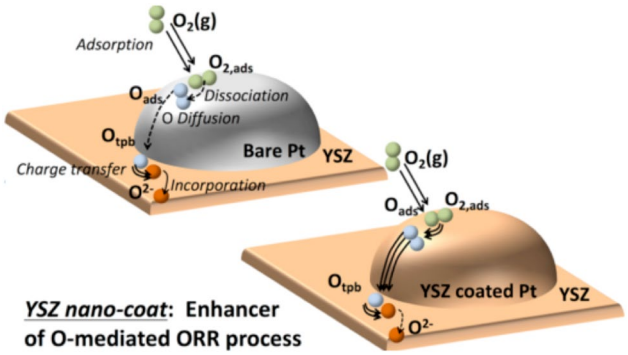

Fig. 12 Schematic diagram depicting the conjectured relative ORR kinetics of bare and YSZ-coated Pt based upon electrochemical analysis. Reproduced with permission from Ref. [87]

In a follow-up report, a mechanistic study was performed to understand the impact of ultrathin ALD coating on catalytic kinetics, especially for ORR on a Pt/YSZ system (Fig. 12) [87]. The ORR process is comprised of its sub-processes. In a Pt/YSZ system, these steps are: adsorption of molecular oxygen on the catalyst surface, dissociation of molecular oxygen into atomic specie-s, surface diffusion of atomic oxygen to the TPB, charge transfer reaction and incorporation of oxygen ions into electrolyte.

By leveraging the differences in oxygen partial pressure ($p(O_2)$) dependency of these sub-processes, it is possible to reveal the rate determining step of ORR. The reaction order m, defined in the relation $R_p^{-1} \propto p(O_2)^m$ (R_p: electrode polarization resistance) provides abundant clues about the rate-limiting step [88]. For example, reaction order of m = 1 indicates that the rate-determining step is likely related to a molecular oxygen-mediated process such as O_2 adsorption and diffusion. A square root $p(O_2)$ dependence (m = ½) corresponds to an atomic oxygen-related process including dissociation into atomic oxygen species and their surface transport, and m = ¼ dependence can be ascribed to a process related to charge transfer reaction [89]. From the dependences on $p(O_2)$, temperature and overpotential, the followings were deduced.

First, the ORR kinetics on a fresh nanoporous Pt/YSZ system is mainly governed by an atomic oxygen-mediated chemical process. After the Pt becomes highly agglomerated during high temperature operation, the rate-limiting step shifted to the charge transfer reaction due to a much smaller TPB area caused by the significant Pt agglomeration. On the other hand, a nanoporous Pt catalyst with a well-dispersed ALD-YSZ overcoat exhibits an ORR process mainly limited by the O^{2-} incorporation or O^{2-} transport through the new Pt/YSZ interfaces formed by the YSZ overcoat while the molecular O_2 adsorption process also plays a considerable rate-determining role especially at a low $p(O_2)$ regime (< 0.1 atm). In short, the YSZ overcoat on Pt can be regarded as a significant facilitator of chemical processes related to atomic oxygen species during ORR in addition to an effective suppressor of Pt agglomeration [87].

A similar approach was taken for Ag-based cathodes of a low temperature SOFC [90, 91]. Li et al. recently reported that an ALD-YSZ treatment on porous Ag cathode with 7–15 cycles resulted in a performance (14.7 mW/cm^2 at 450 °C) comparable to that of a cell with Pt electrode [92]. Several ALD cycles resulted in island-like YSZ particles, while 15 cycle treatment of ALD YSZ showed the uniform film structure on Ag cathode. Figure 13, and they ascribed the enhanced performance to an increase of TPB sites between the Ag surface and ALD-YSZ NPs made by several ALD cycles. The Ag cathode suffered from unwanted coverage of YSZ overcoat with increased ALD cycles, which would lessen TPB sites. While Ag is known to be highly volatile and unstable for SOFC purpose, an ALD-YSZ treatment enabled a significant improvement in thermal stability (Fig. 14). Similar to the result of Li et al., ALD CeO_x treatment on Ag cathode also exhibited an enhanced performance and stability of low temperature SOFCs. Neoh et al. modified the Ag

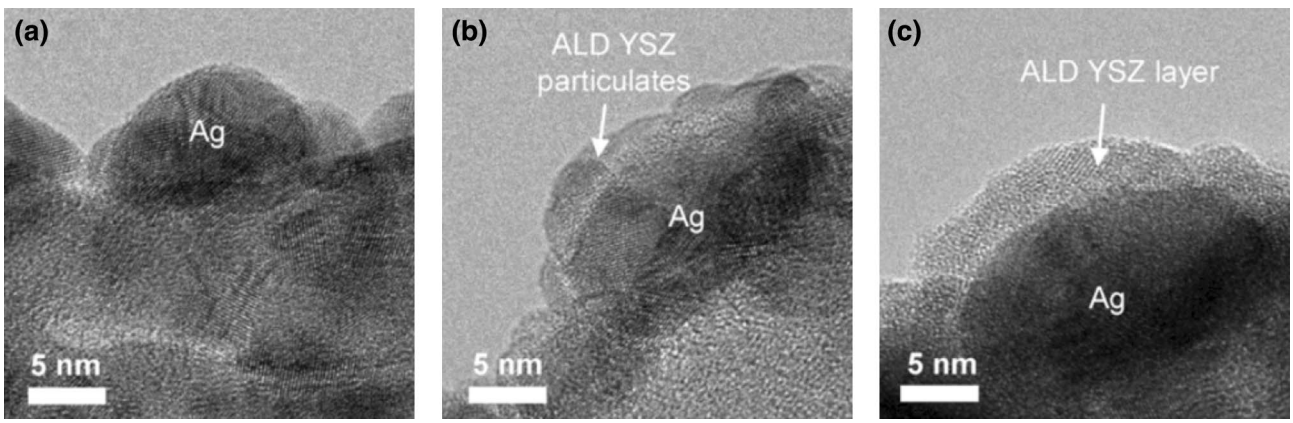

Fig. 13 HRTEM images of **a** bare Ag, **b** Ag-ALD YSZ 7, **c** Ag-ALD YSZ 15 cathodes. Reproduced with permission from Ref. [92]

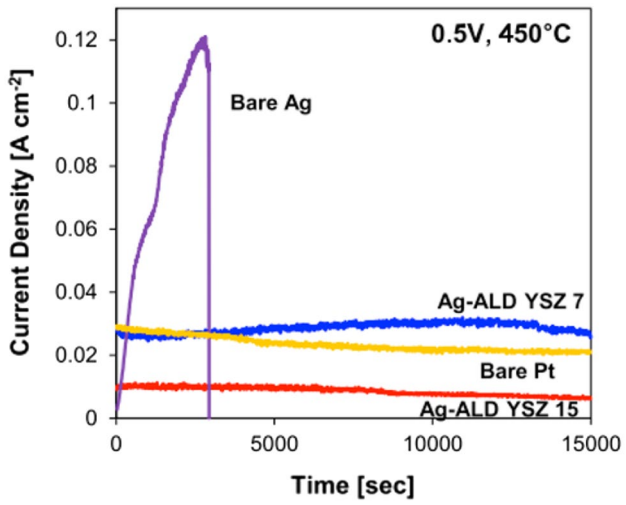

Fig. 14 Evolution of potentiostatic current from cells with bare porous Ag, Pt, and ALD-YSZ-coated Ag (7 and 15 ALD cycles) measured at 0.5 V and 450 °C. Reproduced with permission from Ref. [92]

cathode by ALD CeO_x with different cycle numbers of 2, 5 and 10 [91]. 5 cycle ALD CeO_x treated sample showed the best fuel cell performance at the temperature range of 350–450 °C. Performance enhancement was mainly originated from a decreased polarization loss.

3.4.2 For Perovskite Cathodes

Huang and colleagues recently took a similar ALD-based approach for conventional perovskite-based cathodes. They first presented that a nanoscale ALD ZrO_2 film on $La_{0.6}Sr_{0.4}CoO_3$ (LSC) cathode enabled an exceptional stability of an SOFC for 4000 h at 700 °C [93]. The overall thickness of the ZrO_2 coating was ~ 5 nm. The most pronounced effect of ALD was found in the cathodic polarization resistance (R_p); R_p of the pristine sample increased at a rate of 0.79 Ω cm^2 per 1000 h. In contrast, R_p of the overcoated sample increases at a much smaller rate of 0.04 Ω cm^2 per 1000 h (Fig. 15). First, as was the case for Pt, the ALD overcoat contributed to a geometric confinement significantly, preserving the overall high-surface-area morphology of LSC. Secondly, against the widespread belief that zirconia is detrimental when in direct contact with La and Sr-based cathodes, the ZrO_2 overcoat in this study improved the ORR catalysis by becoming porous and mixed-conducting during operation. Finally, they additionally ascribed the improved performance and durability to a suppression of Sr segregation, one of the widely known cathodic degradation mechanisms. These multi-faceted synergistic effects are believed to improve both cathodic kinetics and durability significantly.

In another report, they applied the same approach to a more conventional SOFC cathode material: $La_{0.6}Sr_{0.4}Fe_{0.8}Co_{0.2}O_{3-\delta}$-$Gd_{0.2}Ce_{0.8}O_{1.9}$ (LSCF-GDC) composite [94]. Over a > 1100 h testing at 800 °C, the overcoated LSCF-GDC hybrid cathode exhibited a polarization and an ohmic area-specific-resistance, 3 and 1.5 times lower than the pristine sample, respectively, with a degradation rate 4 times slower than the pristine counterpart (Fig. 16). In this study, the ZrO_2 overcoat was 20 nm, much thicker than their earlier study.

In a recent report on this topic [95], Gorte and colleagues presented the impact of ALD-based CeO_x and SrO overcoat on the performance of three different hybrid cathodes with YSZ: $La_{0.8}Sr_{0.2}FeO_3$ (LSF), $Ba_{0.5}Sr_{0.5}Co_{0.8}Fe_{0.2}O_3$ (BSCF) and LSC. Unlike Huang et al.'s observation, in which ALD-ZrO_2 overcoat afforded a performance enhancement, both CeO_x and SrO overcoats were found to be detrimental to the cathodic performance [95]. With more ALD cycles (and thus thicker overcoat), a higher polarization resistance resulted (Fig. 17 for CeO_x ALD). While the incorporation of ceria NPs (not by ALD) resulted in an enhanced electrode

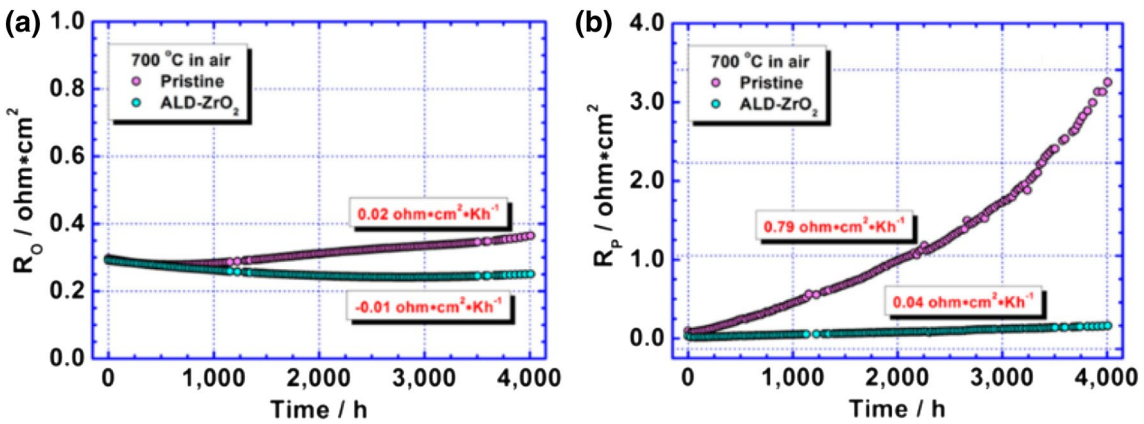

Fig. 15 Long-term stability of a pristine and ALD-ZrO_2 coated LSC cathodes in **a** ohmic resistance and **b** cathodic polarization resistance for 4000 h at 700 °C. Reproduced with permission from Ref. [93]

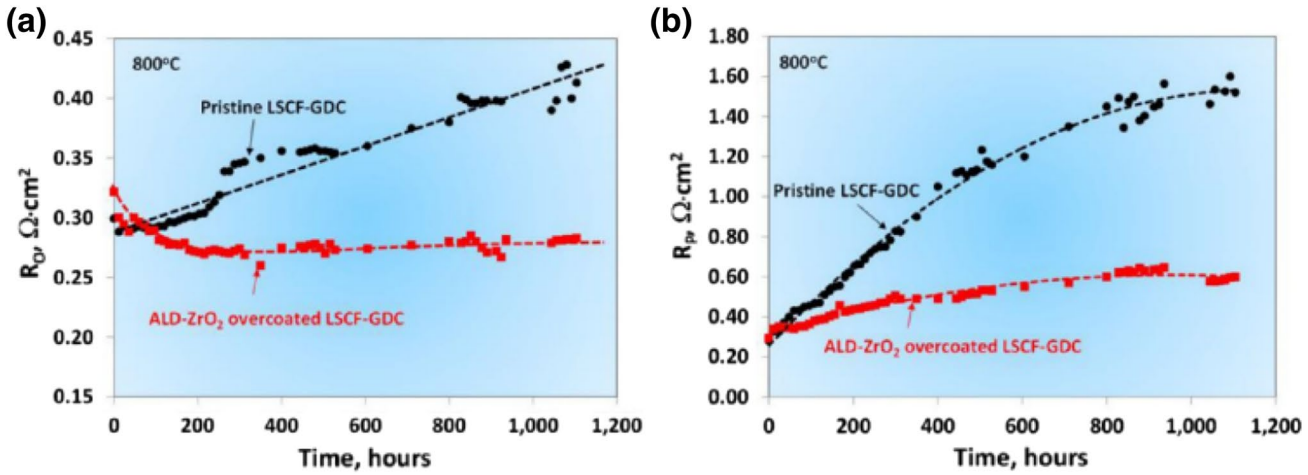

Fig. 16 Long-term stability of a pristine and ALD-ZrO_2 coated LSCF-GDC cathodes in **a** ohmic resistance and **b** cathodic polarization resistance for ~ 1200 h at 800 °C. Reproduced with permission from Ref. [94]

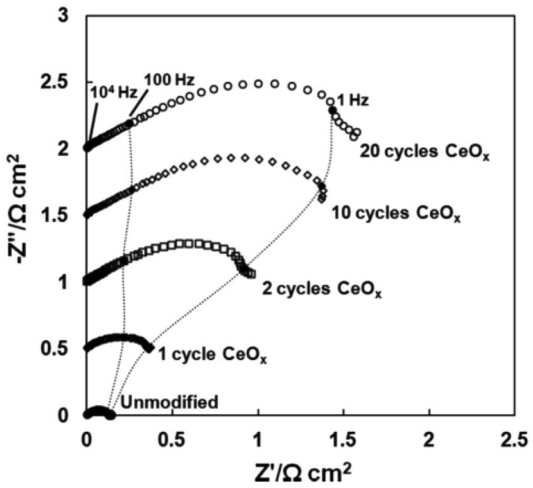

Fig. 17 Nyquist plots of LSF-YSZ cathode symmetric cells calcined to 1123 K and measured at 973 K after CeO_x ALD treatment. Reproduced with permission from Ref. [95]

performance, ALD-based CeO_2 acted as an effective poison. They conjectured it is originated from the fact that the Ce atoms added by ALD are in the +3 oxidation state, causing a decrease in O_2 adsorption by the coating. As the resulting morphology after ALD coating is also significantly different from those after an infiltration of ceria NPs, the actual reason for the differences in electrode performance between the two samples was not revealed clearly. The detrimental impact of ALD-CeO_x overcoat, however, was much less on LSC-YSZ and BSCF-YSZ than on LSF-YSZ. On the other hand, ALD of SrO was found to geometrically block the active surface area. Along with the results proposed by Gorte group, Choi et al. also reported the performance degradation of ALD CoO_x treated LSC cathode [96]. CoO_x coated cell with 30 ALD cycles exhibited a performance degradation. This degradation was ascribed to a partially blocked oxygen surface exchange by the overcoat.

3.5 ALD for Anodes

There have been intense efforts to develop sulfur-tolerant catalysts. While Ni is the most dominant choice for anode, it is the material that is the most susceptible to sulfidation among other anodic alternatives [97]. As noble metals such as Pt, Ru, and Rh exhibit a less thermodynamic stability for sulfidation compared to Ni, they can be a good choice to address the sulfur poisoning issue but at the price of cost competitiveness [98, 99]. In addition, many studies have been reported on Ni-alloy-based catalysts. Most of bimetallic catalysts including Ni-Mo [100], Ni-Co [101], Ni-Rh [102], Ni-La and Ni-Re [103] showed a superior performance compared to bare Ni. Among those, Ni-Mo, Ni-La and Ni-Re exhibited a better resilience against sulfur poisoning. While the reason of better sulfur resistance has not been fully revealed, it can be ascribed to either a sacrificial formation of sulfide by the second component (e.g., Mo acts as a sacrificial agent by readily forming MoS_2 and thus leaving Ni unaffected [100]) or a change in electronic energy barrier against sulfur poisoning (chemical bonding between dissimilar metals resulting in a change of chemical reactivity toward sulfidation) [36]. On the other hand, the role of support materials should not be overlooked. One of the usual approach to address sulfur poisoning is to use a support material with high oxygen mobility such as doped ceria [104–106].

Recently, Jeong et al. utilized ALD to synthesize a bimetallic catalyst for direct alcohol SOFCs (DASOFC) which use ethanol or methanol as the fuel instead of hydrogen [107,

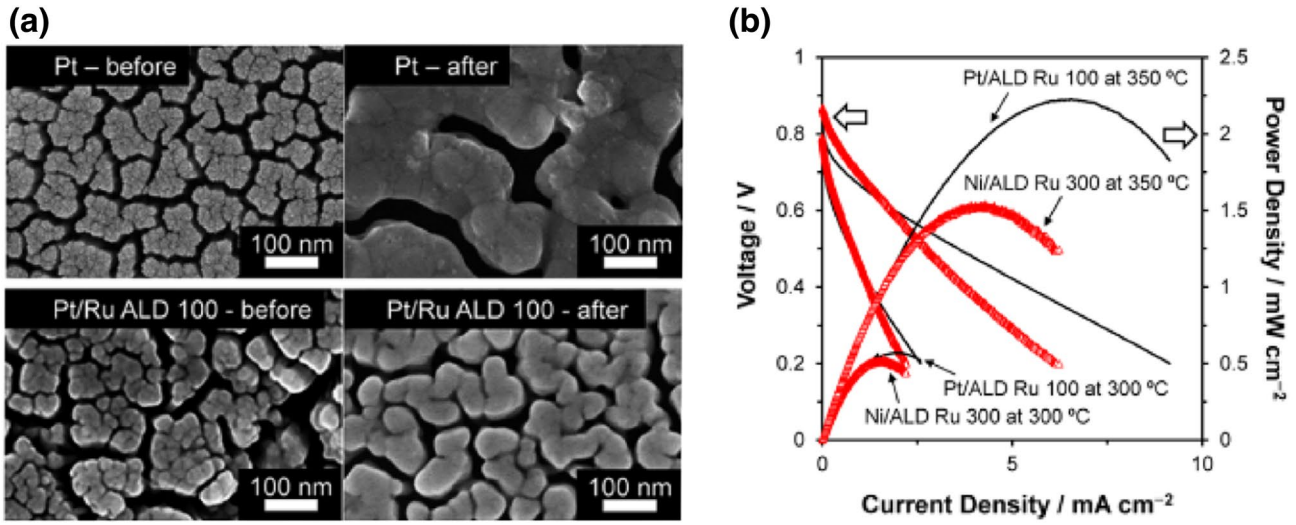

Fig. 18 **a** FESEM image of Pt and Pt/Ru 100 cycle ALD before and after fuel cell operation at 450 °C. **b** Fuel cell performance of Ni/ALD Ru (300 cycles) and Pt/ALD Ru (100 cycles) samples using pure methanol at 300 and 350 °C. Reproduced with permission from Refs. [107] and [108]

108]. Pt anode coated with Ru by ALD showed a significant improvement of anodic activity and powering performance at 300–500 °C [108, 109]. ALD Ru treated samples also showed lower carbon contents on the anode surface and thus an improved operational durability. A bimetallic Ni-Ru anode was also realized by ALD for direct methanol SOFC [107]. Similar to their previous reports on bimetallic Pt-Ru anode catalysts, ALD Ru treated Ni anode showed an enhanced performance and stability. The performance of ALD Ru-treated Pt was interestingly comparable to that of ALD Ru-treated Ni at 300–350 °C although the ALD Ru/Ni sample has a significantly smaller amount of noble metal than the other sample, making it a promising candidate as a high-performance DMSOFC anode material with cost competiveness. In this view, ALD can be a useful tool to synthesize noble metal-based catalysts with maximized specific mass activity (Fig. 18).

4 Conclusion and Perspective

Unique and versatile features of ALD has enabled unprecedented nanoscale engineering for SOFCs in various aspects. The capability of depositing a gas-tight, dense and uniform oxide film enabled high-performance fuel cells working at extremely low operating temperatures by realizing an ultrathin solid electrolyte. The precise thickness control (down to sub-nanometer scale) and conformal coating even on a complex porous geometry (characteristic of conventional electrode backbone) also enabled surface-sensitive treatment of electrode surfaces, which is leveraged for morphological stability, electrochemical kinetics and poisoning resistivity of cells. ALD is also applicable to the interfaces between dissimilar layers in a cell for enhanced charge exchange and reaction kinetics. In this review, these applicability of ALD to SOFCs are discussed by linking representative examples with the unique characteristics of ALD.

While ALD has proven to be an effective approach in many aspects of SOFCs, there are still a significant amount of unprecedented areas and combinations of materials to be probed. More importantly, related fundamental understandings behind the enhanced performance and durability is largely lacking. Currently, most ALD-based SOFC studies stay at a phenomenological level without much of in-depth study, limiting a widespread application of this approach. It is expected significant efforts will be made in this respect on both experimental and theoretical fronts in the upcoming years/decade.

Acknowledgement The authors acknowledge the support from the NSF CAREER Award (DMR 1753383) and the Korea Institute of Industrial Technology (KITECH).

Compliance with ethical standards

Conflict of interest On behalf of all authors, the corresponding author states that there is no conflict of interest.

References

1. Singhal, S. C. (2000). Advances in solid oxide fuel cell technology. *Solid State Ionics, 135*(1–4), 305–313.
2. Jacobson, A. J. (2010). Materials for solid oxide fuel cells. *Chemistry of Materials, 22*(3), 660–674.

3. Steele, B. C., & Heinzel, A. (2001). Materials for fuel-cell technologies. *Nature, 414*(November), 345–352.
4. Ding, D., Li, X., Lai, S. Y., Gerdes, K., & Liu, M. (2014). Enhancing SOFC cathode performance by surface modification through infiltration. *Energy & Environmental Science, 7*(2), 552.
5. Evans, A., Bieberle-Hütter, A., Rupp, J. L. M., & Gauckler, L. J. (2009). Review on microfabricated micro-solid oxide fuel cell membranes. *Journal of Power Sources, 194*(1), 119–129.
6. Hibino, T. (2000). A low-operating-temperature solid oxide fuel cell in hydrocarbon-air mixtures. *Science, 288*(5473), 2031–2033.
7. Wachsman, E. D., & Lee, K. T. (2011). Lowering the temperature of solid oxide fuel cells. *Science New York, 334*(6058), 935–939.
8. Oh, E.-O., Whang, C.-M., Lee, Y.-R., et al. (2012). Extremely thin bilayer electrolyte for solid oxide fuel cells (SOFCs) fabricated by chemical solution deposition (CSD). *Advanced Materials (Deerfield Beach, Fla.), 24*(25), 3373–3377.
9. Shao, Z., & Haile, S. M. (2004). A high-performance cathode for the next generation of solid-oxide fuel cells. *Nature, 431*(7005), 170–173.
10. Yan, N., Xiao, C., & Kou, Y. (2010). Transition metal nanoparticle catalysis in green solvents. *Coordination Chemistry Reviews, 254*(9–10), 1179–1218.
11. Boccuzzi, F., Chiorino, A., & Manzoli, M. (2001). Au/TiO_2 nanostructured catalyst: effects of gold particle sizes on CO oxidation at 90 K. *Materials Science and Engineering C, 15*(1–2), 215–217.
12. Gao, F., & Goodman, D. W. (2012). Model catalysts: Simulating the complexities of heterogeneous catalysts. *Annual Review of Physical Chemistry, 63*(1), 265–286.
13. Kung, M. C., Davis, R. J., & Kung, H. H. (2007). Understanding au-catalyzed low-temperature co oxidation. *The Journal of Physical Chemistry C., 111*(32), 11767–11775.
14. Lim, D. C., Lopez-Salido, I., Dietsche, R., Bubek, M., & Kim, Y. D. (2006). Size-selectivity in the oxidation behaviors of Au nanoparticles. *Angewandte Chemie - International Edition., 45,* 2413–2415.
15. Tsunoyama, H., Sakurai, H., Negishi, Y., & Tsukuda, T. (2005). Size-specific catalytic activity of polymer-stabilized gold nanoclusters for aerobic alcohol oxidation in water. *Journal of the American Chemical Society, 127*(26), 9374–9375.
16. Hayashi, T., Tanaka, K., & Haruta, M. (1998). Selective vapor-phase epoxidation of propylene over Au/TiO_2 catalysts in the presence of oxygen and hydrogen. *Journal of Catalysis, 178,* 566–575.
17. Janssens, T. V. W., Carlsson, A., Puig-Molina, A., & Clausen, B. S. (2006). Relation between nanoscale Au particle structure and activity for CO oxidation on supported gold catalysts. *Journal of Catalysis, 240,* 108–113.
18. De Hosson, J. T. M., & Kooi, B. J. (2001). Metal/ceramic interfaces: a microscopic analysis. *Surface and Interface Analysis, 31*(7), 637–658.
19. Cargnello, M., Delgado Jaén, J. J., Hernández Garrido, J. C., et al. (2012). Exceptional activity for methane combustion over modular Pd@CeO2 subunits on functionalized Al2O3. *Science, 337*(6095), 713–717.
20. Adijanto, L., Sampath, A., Yu, A. S., et al. (2013). Synthesis and stability of Pd@CeO_2 core–shell catalyst films in solid oxide fuel cell anodes. *ACS Catalysis., 3*(8), 1801–1809.
21. Sun, Y.-N., Qin, Z.-H., Lewandowski, M., et al. (2009). Monolayer iron oxide film on platinum promotes low temperature CO oxidation. *Journal of Catalysis, 266*(2), 359–368.
22. Strasser, P., Koh, S., Anniyev, T., et al. (2010). Lattice-strain control of the activity in dealloyed core-shell fuel cell catalysts. *Nature chemistry., 2*(6), 454–460.
23. Ding, H., Virkar, A. V., Liu, M., & Liu, F. (2013). Suppression of Sr surface segregation in $La_{1-x}Sr_xCo_{1-y}Fe_yO_{3-delta}$: a first principles study. *Physical Chemistry Chemical Physics: PCCP, 15*(2), 489–496.
24. Zhao, L., Drennan, J., Kong, C., Amarasinghe, S., & Jiang, S. P. (2014). Insight into surface segregation and chromium deposition on $La_{0.6}Sr_{0.4}Co_{0.2}Fe_{0.8}O_{3-\delta}$ cathodes of solid oxide fuel cells. *J. Mater. Chem. A., 2*(29), 11114–11123.
25. Ponce, S., Peña, M. A., & Fierro, J. L. G. (2000). Surface properties and catalytic performance in methane combustion of SR-substituted lanthanum manganites. *Applied Catalysis, B: Environmental, 24*(3–4), 193–205.
26. Kubicek, M., Limbeck, A., Frömling, T., Hutter, H., & Fleig, J. (2011). Relationship between cation segregation and the electrochemical oxygen reduction kinetics of $La_{0.6}Sr_{0.4}CoO_{3-\delta}$ thin film electrodes. *Journal of the Electrochemical Society, 158*(6), B727.
27. Sase, M., Hermes, F., Yashiro, K., et al. (2008). Enhancement of oxygen surface exchange at the hetero-interface of (La, Sr) CoO3/(La, Sr)2CoO4 with PLD-layered films. *Journal of the Electrochemical Society, 155*(8), B793.
28. Sun, C., Hui, R., & Roller, J. (2009). Cathode materials for solid oxide fuel cells: a review. *Journal of Solid State Electrochemistry, 14*(7), 1125–1144.
29. Druce, J., Téllez, H., & Hyodo, J. (2014). Surface segregation and poisoning in materials for low-temperature SOFCs. *MRS Bulletin, 39*(09), 810–815.
30. Xiong, Y., Yamaji, K., Horita, T., et al. (2009). Sulfur poisoning of SOFC cathodes. *Journal of the Electrochemical Society, 156*(5), B588.
31. Song, C., & Ma, X. (2003). New design approaches to ultra-clean diesel fuels by deep desulfurization and deep dearomatization. In Applied catalysis B: Environmental. pp 207–238
32. Aguilar, L., Zha, S., Cheng, Z., Winnick, J., & Liu, M. (2004). A solid oxide fuel cell operating on hydrogen sulfide (H2S) and sulfur-containing fuels. *Journal of Power Sources, 135*(1–2), 17–24.
33. Liu, M., Wei, G. L., Luo, J. L., Sanger, A. R., & Chuang, K. T. (2003). Use of metal sulfides as anode catalysts in H_2S-Air SOFCs. *Journal of the Electrochemical Society, 150*(8), A1025–A1029.
34. Wei, G.-L., Luo, J.-L., Sanger, A. R., & Chuang, K. T. (2004). High-performance anode for H_2S-air SOFCs. *Journal of the Electrochemical Society, 151*(2), A232–A237.
35. Sasaki, K., Haga, K., Yoshizumi, T., et al. (2011). Chemical durability of solid oxide fuel cells: Influence of impurities on long-term performance. *Journal of Power Sources, 196*(22), 9130–9140.
36. Boldrin, P., Ruiz-Trejo, E., Mermelstein, J., Bermúdez Menéndez, J. M., Ramirez Reina, T., & Brandon, N. P. (2016). Strategies for carbon and sulfur tolerant solid oxide fuel cell materials, incorporating lessons from heterogeneous catalysis. *Chemical Reviews, 116*(22), 13633–13684.
37. Bartholomew, C. H. (2001). Mechanisms of catalyst deactivation. *Applied Catalysis, A: General, 212*(1–2), 17–60.
38. Zhao, S., Wang, Y., Dong, J., et al. (2016). Ultrathin metal–organic framework nanosheets for electrocatalytic oxygen evolution. *Nature Energy., 1,* 16184.
39. Bartholomew, C. H. (1982). Carbon deposition in steam reforming and methanation. *Catalysis Reviews., 24*(1), 67–112.
40. Johnson, R. W., Hultqvist, A., & Bent, S. F. (2014). A brief review of atomic layer deposition: from fundamentals to applications. *Materials Today, 17*(5), 236–246.
41. George, S. M. (2010). Atomic layer deposition: An overview. *Chemical Reviews, 110*(1), 111–131.

42. Lee, Y. H., Chang, I., Cho, G. Y., et al. (2018). Thin film solid oxide fuel cells operating below 600 C: A review. *International Journal of Precision Engineering and Manufacturing-Green Technology., 5*(3), 441–453.
43. Cassir, M., Ringuedé, A., & Niinistö, L. (2010). Input of atomic layer deposition for solid oxide fuel cell applications. *Journal of Materials Chemistry, 20*(41), 8987.
44. Onn, T., Küngas, R., Fornasiero, P., Huang, K., & Gorte, R. (2018). Atomic layer deposition on porous materials: Problems with conventional approaches to catalyst and fuel cell electrode preparation. *Inorganics, 6*(1), 34.
45. Heil, S. B. S., Kudlacek, P., Langereis, E., Engeln, R., van de Sanden, M. C. M., & Kessels, W. M. M. (2006). In situ reaction mechanism studies of plasma-assisted atomic layer deposition of Al2O3. *Applied Physics Letters, 89*(13), 131505.
46. Levy, D. H., Nelson, S. F., & Freeman, D. (2009). Oxide electronics by spatial atomic layer deposition. *Journal of Display Technology., 5*(12), 484–494.
47. Werner, F., Veith, B., Tiba, V., et al. (2010). Very low surface recombination velocities on p- and n-type c-Si by ultrafast spatial atomic layer deposition of aluminum oxide. *Applied Physics Letters, 97*(16), 162103.
48. Poodt, P., Tiba, V., Werner, F., Schmidt, J., Vermeer, A., & Roozeboom, F. (2011). Ultrafast atomic layer deposition of alumina layers for solar cell passivation. *Journal of the Electrochemical Society, 158*(9), H937.
49. Chu, W. S., Kim, M. S., Jang, K. H., et al. (2016). From design for manufacturing (DFM) to manufacturing for design (MFD) via hybrid manufacturing and smart factory: A review and perspective of paradigm shift. *International Journal of Precision Engineering and Manufacturing - Green Technology, 3,* 209–222.
50. Joe, H.-E., Yun, H., Jo, S.-H., Jun, M. B. G., & Min, B.-K. (2018). A review on optical fiber sensors for environmental monitoring. *International Journal of Precision Engineering and Manufacturing-Green Technology., 5*(1), 173–191.
51. Su, P.-C., Chao, C.-C., Shim, J. H., Fasching, R., & Prinz, F. B. (2008). Solid oxide fuel cell with corrugated thin film electrolyte. *Nano Letters, 8*(8), 2289–2292.
52. Shim, J. H., Chao, C., Huang, H., et al. (2007). Atomic layer deposition of Yttria-stabilized zirconia for solid oxide fuel cells. *Chemistry of Materials, 19*(15), 3850–3854.
53. Frison, R., Heiroth, S., Rupp, J. L. M., et al. (2013). Crystallization of 8 mol% yttria-stabilized zirconia thin-films deposited by RF-sputtering. *Solid State Ionics, 232,* 29–36.
54. Tsuchiya, M., Lai, B.-K., & Ramanathan, S. (2011). Scalable nanostructured membranes for solid-oxide fuel cells. *Nature Nanotechnology, 6*(5), 282–286.
55. Kim, H., & Song, H. S. (2014). Design principles of co-planar interdigitated microelectrode arrays for solid-state ionic devices. *International Journal of Precision Engineering and Manufacturing - Green Technology., 1*(4), 317–322.
56. An, J., Kim, Y.-B., Park, J., Gür, T. M., & Prinz, F. B. (2013). Three-dimensional nanostructured bilayer solid oxide fuel cell with 1.3 W/cm2 at 450 C. *Nano Letters, 13*(9), 4551–4555.
57. Baek, J. D., Yu, C.-C., & Su, P.-C. (2016). A silicon-based nanothin film solid oxide fuel cell array with edge reinforced support for enhanced thermal mechanical stability. *Nano Letters, 16*(4), 2413–2417.
58. Ji, S., Cho, G. Y. G. Y., Yu, W., Su, P.-C. P.-C., Lee, M. H. M. H., & Cha, S. W. S. W. (2015). Plasma-enhanced atomic layer deposition of nanoscale yttria-stabilized zirconia electrolyte for solid oxide fuel cells with porous substrate. *ACS Applied Materials & Interfaces, 7*(5), 2998–3002.
59. Ballée, E., Ringuedé, A., Cassir, M., Putkonen, M., & Niinistö, L. (2009). Synthesis of a thin-layered ionic conductor, $CeO_2-Y_2O_3$, by atomic layer deposition in view of solid oxide fuel cell applications. *Chemistry of Materials, 21*(19), 4614–4619.
60. Duan, C., Kee, R. J., Zhu, H., et al. (2018). Highly durable, coking and sulfur tolerant, fuel-flexible protonic ceramic fuel cells. *Nature, 557*(7704), 217–222.
61. Choi, S., Kucharczyk, C. J., Liang, Y., et al. (2018). Exceptional power density and stability at intermediate temperatures in protonic ceramic fuel cells. *Nature Energy., 3*(3), 202–210.
62. Bae, K., Jang, D. Y., Choi, H. J., et al. (2017). Demonstrating the potential of yttrium-doped barium zirconate electrolyte for high-performance fuel cells. *Nature Communications., 8,* 14553.
63. Shim, J. H., Park, J. S., An, J., Gür, T. M., Kang, S., & Prinz, F. B. (2009). Intermediate-temperature ceramic fuel cells with thin film yttrium-doped barium zirconate electrolytes. *Chemistry of Materials, 21*(14), 3290–3296.
64. Li, Y., Wang, S., & Su, P.-C. (2016). Proton-conducting microsolid oxide fuel cells with improved cathode reactions by a nanoscale thin film gadolinium-doped ceria interlayer. *Scientific Reports., 6,* 22369.
65. Liu, Q. L., Khor, K. A., Chan, S. H., & Chen, X. J. (2006). Anode-supported solid oxide fuel cell with yttria-stabilized zirconia/gadolinia-doped ceria bilayer electrolyte prepared by wet ceramic co-sintering process. *Journal of Power Sources, 162*(2), 1036–1042.
66. Zhang, X., Gazzarri, J., Robertson, M., Deces-Petit, C., & Kesler, O. (2008). Stability study of cermet-supported solid oxide fuel cells with bi-layered electrolyte. *Journal of Power Sources, 185*(2), 1049–1055.
67. Lim, H.-T., & Virkar, A. V. (2009). Measurement of oxygen chemical potential in Gd_2O_3-doped ceria-Y_2O_3-stabilized zirconia bi-layer electrolyte, anode-supported solid oxide fuel cells. *Journal of Power Sources, 192*(2), 267–278.
68. Jee, Y., Cho, G. Y. G. Y., An, J., et al. (2014). High performance bi-layered electrolytes via atomic layer deposition for solid oxide fuel cells. *Journal of Power Sources, 253,* 114–122.
69. Kwon, T.-H., Lee, T., & Yoo, H.-I. (2011). Partial electronic conductivity and electrolytic domain of bilayer electrolyte Zr0.84Y0.16O1.92/Ce0.9Gd0.1O1.95. *Solid State Ionics, 195*(1), 25–35.
70. Myung, D.-H., Hong, J., Yoon, K., et al. (2012). The effect of an ultra-thin zirconia blocking layer on the performance of a 1-μm-thick gadolinia-doped ceria electrolyte solid-oxide fuel cell. *Journal of Power Sources, 206,* 91–96.
71. Leskelä, M., & Ritala, M. (2002). Atomic layer deposition (ALD): from precursors to thin film structures. *Thin Solid Films, 409*(1), 138–146.
72. Kilner, J. A., De Souza, R. A., & Fullarton, I. C. (1996). Surface exchange of oxygen in mixed conducting perovskite oxides. *Solid State Ionics, 86*(2), 703–709.
73. Yasuda, I. (1994). Precise determination of the chemical diffusion coefficient of calcium-doped lanthanum chromites by means of electrical conductivity relaxation. *Journal of the Electrochemical Society, 141*(5), 1268.
74. Chao, C.-C., Kim, Y. B., & Prinz, F. B. (2009). Surface modification of yttria-stabilized zirconia electrolyte by atomic layer deposition. *Nano Letters, 9*(10), 3626–3628.
75. Chao, C. C., Park, J. S., Tian, X., Shim, J. H., Gur, T. M., & Prinz, F. B. (2013). Enhanced oxygen exchange on surface-engineered yttria-stabilized zirconia. *ACS Nano, 7*(3), 2186–2191.
76. Fan, Z., An, J., Iancu, A., & Prinz, F. B. (2012). Thickness effects of yttria-doped ceria interlayers on solid oxide fuel cells. *Journal of Power Sources, 218,* 187–191.
77. Fan, Z., Chao, C.-C., Hossein-Babaei, F., & Prinz, F. B. (2011). Improving solid oxide fuel cells with yttria-doped ceria interlayers by atomic layer deposition. *Journal of Materials Chemistry, 21*(29), 10903.

78. Lee, W., & Prinz, F. B. (2014). Localized charge transfer reactions near the Pt-YSZ interfaces using Kelvin probe microscopy. *International Journal of Precision Engineering and Manufacturing-Green Technology., 1*(3), 201–205.
79. Simner, S. P., Anderson, M. D., Coleman, J. E., & Stevenson, J. W. (2006). Performance of a novel La(Sr)Fe(Co)O_3-Ag SOFC cathode. *Journal of Power Sources, 161*(1), 115–122.
80. Qiang, F., Sun, K., Zhang, N., Le, S., Zhu, X., & Piao, J. (2009). Optimization on fabrication and performance of A-site-deficient $La_{0.58}Sr_{0.4}Co_{0.2}Fe_{0.8}O_{3-\delta}$ cathode for SOFC. *Journal of Solid State Electrochemistry, 13*(3), 455–467.
81. Jiang, S. P. (2003). Issues on development of (La, Sr)MnO3 cathode for solid oxide fuel cells. *Journal of Power Sources, 124*(2), 390–402.
82. Ding, D., Liu, M., Liu, Z., et al. (2013). Efficient electro-catalysts for enhancing surface activity and stability of SOFC cathodes. *Advanced Energy Materials, 3*(9), 1149–1154.
83. Ding, D., Zhu, W., Gao, J., & Xia, C. (2008). High performance electrolyte-coated anodes for low-temperature solid oxide fuel cells: Model and experiments. *Journal of Power Sources, 179*(1), 177–185.
84. O'Neill, B. J., Jackson, D. H. K., Lee, J., et al. (2015). Catalyst design with atomic layer deposition. *ACS Catalysis, 5*(3), 1804–1825.
85. Chang, I., Ji, S., Park, J., Lee, M. H., & Cha, S. W. (2015). Ultrathin YSZ coating on Pt cathode for high thermal stability and enhanced oxygen reduction reaction activity. *Advanced Energy Materials, 5*(10), 1402251.
86. Liu, K.-Y. K.-Y., Fan, L., Yu, C.-C., & Su, P.-C. (2015). Thermal stability and performance enhancement of nano-porous platinum cathode in solid oxide fuel cells by nanoscale ZrO2 capping. *Electrochemistry Communications, 56,* 65–69.
87. Karimaghaloo, A., Andrade, A. M., Grewal, S., Shim, J. H., & Lee, M. H. (2017). Mechanism of cathodic performance enhancement by a few-nanometer-thick oxide overcoat on porous Pt cathodes of solid oxide fuel cells. *ACS Omega., 2*(3), 806–813.
88. Takeda, Y. (1987). Cathodic polarization phenomena of perovskite oxide electrodes with stabilized zirconia. *Journal of the Electrochemical Society, 134*(11), 2656.
89. Escudero, M. J., Aguadero, A., Alonso, J. A., & Daza, L. (2007). A kinetic study of oxygen reduction reaction on La_2NiO_4 cathodes by means of impedance spectroscopy. *Journal of Electroanalytical Chemistry, 611*(1–2), 107–116.
90. Li, Y. K., Choi, H. J., Kim, H. K., et al. (2015). Nanoporous silver cathodes surface-treated by atomic layer deposition of Y:ZrO_2 for high-performance low-temperature solid oxide fuel cells. *Journal of Power Sources, 295,* 175–181.
91. Neoh, K. C., Han, G. D., Kim, M., et al. (2016). Nanoporous silver cathode surface treated by atomic layer deposition of CeOx for low-temperature solid oxide fuel cells. *Nanotechnology, 27*(18), 185403.
92. Zhou, K., Fan, X., Wei, X., & Liu, J. (2017). The strategies of advanced cathode composites for lithium-sulfur batteries. *Science China Technological Sciences., 60*(2), 175–185.
93. Gong, Y., Palacio, D., Song, X., et al. (2013). Stabilizing nanostructured solid oxide fuel cell cathode with atomic layer deposition. *Nano Letters, 13*(9), 4340–4345.
94. Gong, Y., Patel, R. L., Liang, X., et al. (2013). Atomic layer deposition functionalized composite SOFC cathode La0.6Sr0.4Fe0.8Co0.2O3-δ -Gd0.2Ce0.8O1.9: Enhanced Long-Term Stability. *Chemistry of Materials, 25*(21), 4224–4231.
95. Yu, A. S., Kungas, R., Vohs, J. M., & Gorte, R. J. (2013). Modification of SOFC cathodes by atomic layer deposition. *Journal of the Electrochemical Society, 160*(11), F1225–F1231.
96. Choi, H. J., Bae, K., Jang, D. Y., Kim, J. W., & Shim, J. H. (2015). Performance degradation of lanthanum strontium cobaltite after surface modification. *Journal of the Electrochemical Society, 162*(6), F622–F626.
97. Sehested, J. (2006). Four challenges for nickel steam-reforming catalysts. *Catalysis Today, 111*(1–2), 103–110.
98. Xie, C., Chen, Y., Engelhard, M. H., & Song, C. (2012). Comparative study on the sulfur tolerance and carbon resistance of supported noble metal catalysts in steam reforming of liquid hydrocarbon fuel. *ACS Catalysis., 2*(6), 1127–1137.
99. Von Deak, D., Singh, D., Biddinger, E. J., et al. (2012). Investigation of sulfur poisoning of CNx oxygen reduction catalysts for PEM fuel cells. *Journal of Catalysis, 285,* 145–151.
100. González, M. G., Ponzi, E. N., Ferretti, O. A., Quincoces, C. E., Marecot, P., & Barbier, J. (2000). Studies on H_2S adsorption and carbon deposition over Mo-Ni/Al_2O_3 catalysts. *Adsorption Science & Technology, 18*(6), 541–550.
101. Niakolas, D. K. (2014). Sulfur poisoning of Ni-based anodes for solid oxide fuel cells in H/C-based fuels. *Applied Catalysis, A: General, 486,* 123–142.
102. Xie, C., Chen, Y., Li, Y., Wang, X., & Song, C. (2010). Sulfur poisoning of CeO_2-Al_2O_3-supported mono- and bi-metallic Ni and Rh catalysts in steam reforming of liquid hydrocarbons at low and high temperatures. *Applied Catalysis, A: General, 390*(1–2), 210–218.
103. Murata, K., Saito, M., Inaba, M., & Takahara, I. (2007). Hydrogen production by autothermal reforming of sulfur-containing hydrocarbons over Re-modified Ni/Sr/ZrO2 catalysts. *Applied Catalysis, B: Environmental, 70*(1–4), 509–514.
104. Gorte, R. J. (2010). Ceria in catalysis: From automotive applications to the water-gas shift reaction. *AIChE Journal, 56*(5), 1126–1135.
105. Luo, T. (2002). An examination of sulfur poisoning on Pd/ceria catalysts. *Journal of Catalysis, 210*(2), 397–404.
106. Andreeva, D., Ivanov, I., Ilieva, L., Sobczak, J. W., Avdeev, G., & Petrov, K. (2007). Gold based catalysts on ceria and ceria-alumina for WGS reaction (WGS Gold catalysts). *Topics in Catalysis, 44*(1–2), 173–182.
107. Jeong, H., Kim, J. W., Park, J., et al. (2016). Bimetallic nickel/ruthenium catalysts synthesized by atomic layer deposition for low-temperature direct methanol solid oxide fuel cells. *ACS Applied Materials & Interfaces, 8*(44), 30090–30098.
108. Jeong, H. J., Kim, J. W., Bae, K., Jung, H., & Shim, J. H. (2015). Platinum–ruthenium heterogeneous catalytic anodes prepared by atomic layer deposition for use in direct methanol solid oxide fuel cells. *ACS Catalysis., 5*(3), 1914–1921.
109. Jeong, H. J., Kim, J. W., Jang, D. Y., & Shim, J. H. (2015). Atomic layer deposition of ruthenium surface-coating on porous platinum catalysts for high-performance direct ethanol solid oxide fuel cells. *Journal of Power Sources, 291,* 239–245.

Alireza Karimaghaloo is currently a Ph.D. candidate in the Department of Mechanical Engineering at UC Merced. His research interests include atomic layer deposition (ALD) and nano-characterization of fuel cells.

Junmo Koo is a Ph.D. candidate in the School of Mechanical Engineering, Korea University. His research interests are artificial neural network and atomic layer deposition.

Joon Hyung Shim is an Associate Professor in the School of Mechanical Engineering at Korea University (KU) and a director of Makerspace at KU. His research interests are smart grid simulation of renewable energy systems, development of high-performance fuel cells, and characterization of thin-film-based devices.

Hung-Sen Kang received his MS with honors in applied physics at National Taiwan University in 2012 and he is currently a Ph.D. candidate in the Department of Mechanical Engineering at University of California, Merced. His research interests include nanoscale fuel cells and atomic force microscopy-cased observations.

Min Hwan Lee is an Assistant Professor in the Department of Mechanical Engineering at the University of California, Merced. He obtained his Ph.D. in Mechanical Engineering from Stanford University. His research interests include development of high-performance and durable fuel cells via nanoscale materials engineering, and nanoscale analysis of underpinning catalysis.

Shin Ae Song is currently a senior researcher at Micro/Nano Scale Manufacturing Group of Korea Institute of Industrial Technology. She received her Ph.D. in chemical engineering at KAIST (Korea Advanced Institute of Science and Technology) in South Korea in 2009. Her research interests include electrodes and electrolyte for molten carbonate fuel cells and solid oxide fuel cells.